Time-dependent coupled-channel calculations of positronium-formation cross sections in positron-hydrogen collisions

Nobuhiro Yamanaka*
Department of Physics, University of Tokyo, Tokyo 113-0033, Japan

Yasushi Kino†
Department of Chemistry, Tohoku University, Sendai 980-8578, Japan
(Received 5 April 2001; published 17 September 2001)

We demonstrate the usefulness of the time-dependent coupled channel (TDCC) method in theoretical studies of atomic rearrangement collisions. In the TDCC method, coupled-channel partial differential equations for scattering wave functions are solved time dependently. We develop the Hankel-interpolation method, which is used to transform wave functions from an initial coordinate to a final coordinate system. By using this method, reaction cross sections of rearrangement collisions can be directly extracted from solutions of TDCC equations. We calculate positronium-formation cross sections in positron-hydrogen collisions in which a considerable number of theoretical calculations and precise experiments have been made. The present results for positron energies of 6.8–35 eV are in excellent agreement with the recent experiment of Zhou *et al.* [Phys. Rev. A **55**, 361 (1997)].

DOI: 10.1103/PhysRevA.64.042715 PACS number(s): 34.70.+e, 36.10.Dr

I. INTRODUCTION

Positronium (Ps) formation by positron-hydrogen collisions is one of the simplest systems of atomic rearrangement collisions. It provides a testing ground for theoretical models used to study more complex rearrangement reactions (see, for example, Refs. [1,2] and references therein). Beside, precise experiments recently made by Weber *et al.* [3] and Zhou *et al.* [4] stimulate theoretical studies of the Ps formation. However, treatment of the Ps formation is intrinsically difficult in comparison with that of ionization and excitation of the hydrogen by positron collisions, since different coordinate systems must be used to describe the three-body system before and after the rearrangement collision. Hence, previous theoretical models were available only for low energies at which a few channels are open. For positron energies of 6.8–10.2 eV (Ore gap), Humberston *et al.* [5] calculated Ps-formation cross sections using the Kohn-variational method, and Kar and Mandal [6] using the Schwinger-variational method. Higgins and Burke [7] employed the *R*-matrix method, Liu and Gien and Kuang and Gien [8] and Mitroy *et al.* [9] close-coupling methods, Ward *et al.* [10] the hidden-crossing method, and Janev and Solov'ev [11] the advanced adiabatic method. The results of these calculations agree with each other in a low-energy region.

For intermediate or high energies at which many channels are open, Hewitt *et al.* [12], Mitroy and Stelbovics [13], McAlinden *et al.* [14], Gien [15], and Sarkar and Ghosh [16] used close-coupling methods. However, unphysical resonances were found in Ps-formation cross sections, since atomic-type basis functions used were over complete and hydrogen and Ps components of the total wave functions were not orthogonal. The resonances have not been obtained with a hyperspherical close-coupling method as reported by Igarashi and Toshima [17] and Zhou and Lin [18]. Mitroy [19] and Kernoghan *et al.* [20] avoided the problem of the over completeness by decreasing the number of Ps-formation channels; only the $1s$, $2s$, and $2p$ states of Ps were included. Other excited states were not included, even if they were open channels. However, this treatment is not proper in intermediate energies where contribution of Ps-formation channels becomes important.

One of the promising approaches to overcome the problem of the over completeness is to time-dependently solve coupled-channel partial differential equations for scattering wave functions, i.e., the time-dependent coupled-channel (TDCC) method [21]. In this approach, a wave packet that describes relative motions in a three-body system is time evolved on a lattice of the two-dimensional radial space. Hence, a physical picture of dynamics can be easily obtained within a full-quantal framework through a computer graphics. Another advantage is that no asymptotic boundary condition is required on wave functions. As a result, Ps formation and ionization channels need not be separately included. In addition, by numerically describing wave functions, the number of channels can drastically decrease. Thus, the TDCC method is expected to be useful for rearrangement collisions in which many channels open. Ihra *et al.* [22], Pindzola *et al.* [23], and Odero *et al.* [24] applied this method to electron-atom collisions, Pindzola and Robicheaux [25] to photo-ionization of atoms, and Schultz *et al.* [26] to atomic auto-ionization.

Recently, Plante and Pindzola [27] applied the TDCC method to the Ps formation. In their calculation, Ps-formation cross sections were deduced from transfer-ionization (Ps formation plus ionization) cross sections obtained with the TDCC method by subtracting ionization cross sections calculated with a lowest-order distorted-wave method. However, the distorted-wave method is not a good

*Email address: yam@nucl.phys.s.u-tokyo.ac.jp
†Email address: kino@mail.cc.tohoku.ac.jp

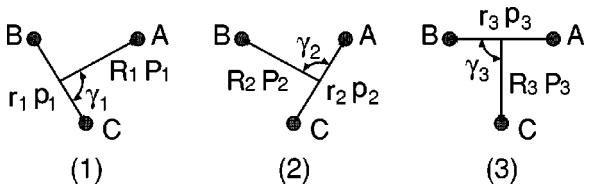

FIG. 1. Jacobi coordinate systems ($c=1$, 2, and 3) corresponding to arrangements of $A+BC$, $B+CA$, and $C+AB$; $\boldsymbol{P}_c$ and $\boldsymbol{p}_c$ are the conjugate momenta of the relative position vectors $\boldsymbol{R}_c$ and $\boldsymbol{r}_c$ and γ_c is the angle between $\hat{\boldsymbol{R}}_c$ and $\hat{\boldsymbol{r}}_c$.

approximation for low energies in which correlation effects are important. In fact, they reported results only for energies higher than 30 eV.

In the present paper, we demonstrate the usefulness of the TDCC method in theoretical studies of atomic rearrangement collisions. First, we develop a fast and stable TDCC method, employing a split-operator method in which the unitary transformation of potential operators and the Cayley expansion of kinetic energy operators are incorporated. TDCC equations can be fast and stably solved on a parallel-computing scheme with an adhesive-operator method. Next, we develop the Hankel interpolation method to transform wave functions in the initial coordinate system, which describes the positron-hydrogen system, to those in the final system, which describes the proton-Ps system. By using this method, Ps-formation cross sections can be directly extracted from solutions of TDCC equations. For positron energies of 6.8–50 eV, we calculate Ps-formation cross sections and compare with the experiments and the previous calculations.

In the present paper, the atomic units ($e=\hbar=m_e=1$) are used unless otherwise stated.

II. TDCC EQUATIONS

We derive TDCC equations for three-body collision systems that consist of A-, B-, and C-particles. Relative motions between the three particles are described in a Jacobi coordinate system ($\boldsymbol{R}_c,\boldsymbol{r}_c$), where $c=1$, 2, or 3, illustrated in Fig. 1. In the figure, γ_c is the angle between $\hat{\boldsymbol{R}}_c$ and $\hat{\boldsymbol{r}}_c$, and $\boldsymbol{P}_c$ and $\boldsymbol{p}_c$ are the conjugate momenta of $\boldsymbol{R}_c$ and $\boldsymbol{r}_c$. For example, the ($c=1$) coordinate system describes an arrangement ($A+BC$) of free states of the A particle and the subsystem of the B and C particles. The Hamiltonian is given by

$$\hat{H}=\frac{1}{2M_1}\hat{\boldsymbol{P}}_1^2+\frac{1}{2\mu_1}\hat{\boldsymbol{p}}_1^2+\hat{V} \tag{2.1}$$

with the interaction operator,

$$\hat{V}=\frac{Z_BZ_C}{r_1}+\frac{Z_AZ_B}{|\boldsymbol{R}_1+[\mu_1/m_B]\boldsymbol{r}_1|}+\frac{Z_AZ_C}{|\boldsymbol{R}_1-[\mu_1/m_C]\boldsymbol{r}_1|}, \tag{2.2}$$

where Z_i and m_i are the charge and mass of the particles ($i=A$, B, or C), and M_1 and μ_1 are the reduced masses,

$$M_1=\frac{m_A(m_B+m_C)}{m_A+m_B+m_C},\quad \mu_1=\frac{m_Bm_C}{m_B+m_C}.$$

The eigenfunction of the Hamiltonian is written in a form

$$\Psi^{JM_J\pi}(\boldsymbol{R}_1,\boldsymbol{r}_1,t)=\frac{1}{R_1r_1}\sum_{lK}\psi_{lK}^{JM_J\pi}(R_1,r_1,t)\mathcal{Y}_{lK}^{JM_J\pi}(\hat{\boldsymbol{R}}_1,\hat{\boldsymbol{r}}_1). \tag{2.3}$$

The parity adapted angular momentum function is defined in the body-fixed (BF) frame as

$$\mathcal{Y}_{lK}^{JM_J\pi}(\hat{\boldsymbol{R}},\hat{\boldsymbol{r}})=\frac{1}{\sqrt{2(1+\delta_{K0})}}[\mathcal{Y}_{lK}^{JM_J}(\hat{\boldsymbol{R}},\hat{\boldsymbol{r}})+(-)^{J+\pi}\mathcal{Y}_{l-K}^{JM_J}(\hat{\boldsymbol{R}},\hat{\boldsymbol{r}})] \tag{2.4}$$

with

$$\mathcal{Y}_{lK}^{JM_J}(\hat{\boldsymbol{R}},\hat{\boldsymbol{r}})=\sqrt{\frac{2J+1}{4\pi}}D_{KM_J}^J(\hat{\boldsymbol{R}})Y_{lK}(\gamma,0), \tag{2.5}$$

where J is the total angular momentum, l the orbital angular momentum associated with $\hat{\boldsymbol{r}}$, K the projection of l on $\hat{\boldsymbol{R}}$, π the parity, $D_{KM_J}^J$ the Wigner rotation matrix, and Y_{lK} the spherical harmonics. The projection quantum number has values of $K=K_{\min}^{\pi}-\min(J,l)$, where $K_{\min}^{\pi}=0$ for $\pi=$even and $K_{\min}^{\pi}=1$ for $\pi=$odd. The expansion (2.3) is substituted into the time-dependent Schrödinger equation,

$$i\frac{\partial}{\partial t}\Psi^{JM_J\pi}(\boldsymbol{R}_1,\boldsymbol{r}_1,t)=\hat{H}\Psi^{JM_J\pi}(\boldsymbol{R}_1,\boldsymbol{r}_1,t). \tag{2.6}$$

The rotation matrix and the spherical harmonics are eliminated by projecting Eq. (2.4) from the left-hand side of Eq. (2.6). This gives the TDCC equation

$$i\frac{\partial}{\partial t}\psi_{lK}^{JM_J\pi}(R_1,r_1,t)=\sum_{l'K'}\left[\hat{T}_{KlK'}^{JM_J\pi}+\frac{\hat{W}_{lKl'K'}^{JM_J\pi}}{2M_1R_1^2}+\frac{l(l+1)}{2\mu_1r_1^2}\delta_{ll'}\delta_{KK'}+\hat{V}_{lKl'K'}^{JM_J\pi}\right]\times\psi_{l'K'}^{JM_J\pi}(R_1,r_1,t), \tag{2.7}$$

where

$$\hat{T}_{lKl'K'}^{JM_J\pi}=\left[-\frac{1}{2M_1}\frac{\partial^2}{\partial R_1^2}-\frac{1}{2\mu_1}\frac{\partial^2}{\partial r_1^2}\right]\delta_{ll'}\delta_{KK'}, \tag{2.8}$$

$$\hat{W}_{lKl'K'}^{JM_J\pi}=[J(J+1)-2K^2+l(l+1)]\delta_{ll'}\delta_{KK'}-\lambda_{JK}^{+}\lambda_{lK}^{+}\sqrt{1+\delta_{K0}}\delta_{ll'}\delta_{K+1K'}-\lambda_{JK}^{-}\lambda_{lK}^{-}\sqrt{1+\delta_{K1}}\delta_{ll'}\delta_{K-1K'}, \tag{2.9}$$

$$\lambda_{lm}^{\pm}=\sqrt{l(l+1)-m(m\pm1)}, \tag{2.10}$$

and

$$\hat{V}_{lKl'K'}^{JM_J\pi}=\langle\mathcal{Y}_{lK}^{JM_J\pi}|\hat{V}|\mathcal{Y}_{l'K'}^{JM_J\pi}\rangle\delta_{KK'}. \tag{2.11}$$

In the BF frame, the TDCC equation can be efficiently solved, since $\hat{T}^{JM_J\pi}_{lKl'K'}$ is diagonal in l and K, $\hat{W}^{JM_J\pi}_{lKl'K'}$ in l, and $\hat{V}^{JM_J\pi}_{lKl'K'}$ in K.

The radial part of the wave function (2.3) in the BF representation is transformed into the radial function $\chi^{JM_J}_{Ll}$ in the space-fixed (SF) representation through a relation

$$\chi^{JM_J}_{Ll}=\sum_K \sqrt{2-\delta_{K0}}\sqrt{\frac{2L+1}{2J+1}}C^{JK}_{lK,L0}\psi^{JM_J\pi}_{lK}, \quad (2.12)$$

and *vice versa*

$$\psi^{JM_J\pi}_{lK}=\sum_L \sqrt{2-\delta_{K0}}\sqrt{\frac{2L+1}{2J+1}}C^{JK}_{lK,L0}\chi^{JM_J}_{Ll}, \quad (2.13)$$

where L is the orbital angular momentum associated with $\hat{\boldsymbol{R}}$ and $C^{JK}_{lK,L0}$ is the Clebsch-Gordan coefficient.

III. FAST AND STABLE SOLUTION OF TDCC EQUATIONS

We present a fast and stable solution of TDCC equations, for simplicity, in an one-dimensional problem,

$$i\frac{\partial}{\partial t}\psi_l(r,t)=\hat{H}_{ll'}\psi_{l'}(r,t). \quad (3.1)$$

Here, we use Einstein's convention of the summation, $a_{ll'}b_{l'}=\Sigma_{l'}a_{ll'}b_{l'}$. Solutions of Eq. (3.1) are written in the form

$$\psi_l(r,t)=\hat{S}_{ll'}(t-t_0)\psi_{l'}(r,t_0), \quad (3.2)$$

with the time-evolution operator

$$\hat{S}_{ll'}(t-t_0)=\exp[-i\hat{H}_{ll'}(t-t_0)]. \quad (3.3)$$

The wave function is discretized on the time space with respect to a short time step $\Delta t=t_{\max}/M$,

$$\psi^{(m)}_l(r)=\psi_l(r,t_m), \quad t_m=m\Delta t, \quad m=0,1,\ldots,M.$$

Solutions of Eq. (3.1) are obtained through iterations

$$\psi^{(m+1)}_l(r)=\hat{S}_{ll'}(\Delta t)\psi^{(m)}_{l'}(r), \quad (3.4)$$

where $\hat{S}_{ll'}(\Delta t)=\exp(-i\hat{H}_{ll'}\Delta t)$.

We consider the Hamiltonian operator in the time-evolution operator. For convenience, the Hamiltonian $\hat{H}_{ll'}$ consists of a nonlocal operator $\hat{T}_{ll'}$ and a local operator $\hat{V}_{ll'}$. With use of the Baker-Campbell-Hausdorff relation, the two operators are separated into the symmetric form [28–30],

$$\hat{S}_{ll'}(\Delta t)=\exp\left(-i\frac{\Delta t}{2}\hat{V}_{ll'}\right)\exp(-i\Delta t\hat{T}_{ll'})\exp\left(-i\frac{\Delta t}{2}\hat{V}_{ll'}\right)+\mathcal{O}(\Delta t^3). \quad (3.5)$$

By using this relation, Eq. (3.4) is separated into three equations,

$$\psi^{(m+1)}_l(r)=\exp\left(-i\frac{\Delta t}{2}\hat{V}_{ll'}\right)\psi^{(m+2/3)}_{l'}(r), \quad (3.6)$$

$$\psi^{(m+2/3)}_l(r)=\exp(-i\Delta t\hat{T}_{ll'})\psi^{(m+1/3)}_{l'}(r), \quad (3.7)$$

$$\psi^{(m+1/3)}_l(r)=\exp\left(-i\frac{\Delta t}{2}\hat{V}_{ll'}\right)\psi^{(m)}_{l'}(r). \quad (3.8)$$

First, we consider calculation of Eq. (3.8) which includes the local operator $\hat{V}_{ll'}$. The operator includes all of the nondiagonal operators; the centrifugal potential operators (2.9) and the second term in Eq. (2.7), and the interaction operators (2.11). With use of a unitary transformation matrix U, the operator $\hat{V}_{ll'}$ is transformed to a diagonal operator $\hat{D}_{ll'''}=U^{\dagger}_{ll'}\hat{V}_{l'l''}U_{l''l'''}$, where $\hat{D}_{ll'}=0$ for $l\neq l'$. Thus, solutions of Eq. (3.8) are obtained through three steps,

$$\psi^{(m+1/3)}_l(r)=U_{ll'}\psi^{(m+2/9)}_{l'}(r), \quad (3.9)$$

$$\psi^{(m+2/9)}_l(r)=\exp\left(-i\frac{\Delta t}{2}\hat{D}_{ll'}\delta_{ll'}\right)\psi^{(m+1/9)}_{l'}(r), \quad (3.10)$$

$$\psi^{(m+1/9)}_l(r)=U^{\dagger}_{ll'}\psi^{(m)}_{l'}(r). \quad (3.11)$$

Calculations of the intermediated functions $\psi^{(m+1/3)}_l$ with Eqs. (3.9), (3.10), and (3.11) nonconditionally stabilize, since the absolute values of the unitary transform matrix and the exponential operator are unity.

Next, we consider calculations of Eq. (3.7). The nonlocal operator $\hat{T}_{ll'}$ that includes the kinetic-energy operators (2.8) is diagonal, i.e., $\hat{T}_{ll'}=0$ for $l\neq l'$. As an example, we define $\hat{T}_{ll'}=-(1/2\mu)\partial^2_r\delta_{ll'}$. The exponential operator with $\hat{T}_{ll'}$ is expanded into Cayley's fractional form [31,32],

$$\exp(-i\Delta t\hat{T}_{ll'})=\exp\left(i\Delta t\frac{\partial^2_r}{2\mu}\delta_{ll'}\right)=\frac{1+i\Delta t\frac{\partial^2_r}{4\mu}\delta_{ll'}}{1-i\Delta t\frac{\partial^2_r}{4\mu}\delta_{ll'}}+\mathcal{O}(\Delta t^3). \quad (3.12)$$

The Cayley expansion is correct to order Δt^2. By substituting Eq. (3.12) into Eq. (3.7) and moving the denominator to the left-hand side, we have

$$\left(1-i\Delta t\frac{\partial^2_r}{4\mu}\right)\psi^{(m+2/3)}_l(r)=\left(1+i\Delta t\frac{\partial^2_r}{4\mu}\right)\psi^{(m+1/3)}_l(r). \quad (3.13)$$

Calculations of the intermediate functions $\psi^{(m+2/3)}_l$ nonconditionally stabilize, since the absolute value of the Cayley expanded operator, the first term in Eq. (3.12), is unity.

Equation (3.13) is often solved with the Crank-Nicholson scheme [31,32]. In the alternative direction implicit (ADI) method, Kono *et al.* [33] employed the Peaceman-Rachfold

scheme and Kawata *et al.* [34] employed the D'yakonov scheme. We employ the modified Cholesky method [35]. The wave function is numerically described on grid points of the r space,

$$\psi_{l,n}^{(m)}=\psi_l^{(m)}(r_n), \quad r_n=n\Delta r, \quad n=0,1,\ldots,N,$$

where $\Delta r=r_{\max}/N$. The differential operator is approximated with the three-point finite difference method. As a result, Eq. (3.13) becomes a simultaneous linear equation;

$$\left[I-i\frac{\Delta t}{4\mu\Delta x^2}\begin{pmatrix} -2 & 1 & 0 & \cdots & 0 & 0 \\ 1 & -2 & 1 & & 0 & 0 \\ 0 & 1 & -2 & & 0 & 0 \\ \vdots & & & \ddots & & \vdots \\ 0 & 0 & 0 & & -2 & 1 \\ 0 & 0 & 0 & \cdots & 1 & -2 \end{pmatrix}\right] \times\begin{pmatrix} \psi_{l,1}^{(m+2/3)} \\ \psi_{l,2}^{(m+2/3)} \\ \psi_{l,3}^{(m+2/3)} \\ \vdots \\ \psi_{l,N-2}^{(m+2/3)} \\ \psi_{l,N-1}^{(m+2/3)} \end{pmatrix}=\begin{pmatrix} \psi_{l,1}^{(m+1/3)*} \\ \psi_{l,2}^{(m+1/3)*} \\ \psi_{l,3}^{(m+1/3)*} \\ \vdots \\ \psi_{l,N-2}^{(m+1/3)*} \\ \psi_{l,N-1}^{(m+1/3)*} \end{pmatrix}, \tag{3.14}$$

where I is the unit matrix and $\psi_l^{(m+1/3)*}$ is the right-hand side of Eq. (3.13). The values of $\psi_{l,0}^{(m+2/3)}$, $\psi_{l,N}^{(m+2/3)}$, $\psi_{l,0}^{(m+1/3)*}$, and $\psi_{l,N}^{(m+1/3)*}$ are fixed to be zero by the boundary condition. The unknown function $\psi_l^{(m+2/3)}$ is efficiently calculated with the modified Cholesky method, since the finite difference matrix is a symmetric-band matrix with the width of unity.

The simultaneous linear equation (3.14) can be calculated also on a parallel computing scheme with an adhesive-operator method [36]. The exponential operator (3.12) is decomposed to be

$$\exp\left(i\Delta t\frac{\partial_r^2}{2\mu}\delta_{ll'}\right)=\exp\left(i\Delta t\frac{\partial_{\rm rad}^2}{4\mu}\delta_{ll'}\right)\exp\left(i\Delta t\frac{\partial_{\rm rbd}^2}{2\mu}\delta_{ll'}\right) \times\exp\left(i\Delta t\frac{\partial_{\rm rad}^2}{4\mu}\delta_{ll'}\right)+\mathcal{O}(\Delta t^3), \tag{3.15}$$

where $\partial_r^2=\partial_{\rm rbd}^2+\partial_{\rm rad}^2$. By expanding the three exponential functions into Cayley's forms similar to Eq. (3.12), Eq. (3.13) is decomposed into a set of three equations;

$$\left(1-i\Delta t\frac{\partial_{\rm rad}^2}{8\mu}\right)\psi_l^{(m+2/3)}(r)=\left(1+i\Delta t\frac{\partial_{\rm rad}^2}{8\mu}\right)\psi_l^{(m+5/9)}(r), \tag{3.16}$$

$$\left(1-i\Delta t\frac{\partial_{\rm rbd}^2}{4\mu}\right)\psi_l^{(m+5/9)}(r)=\left(1+i\Delta t\frac{\partial_{\rm rbd}^2}{4\mu}\right)\psi_l^{(m+4/9)}(r), \tag{3.17}$$

$$\left(1-i\Delta t\frac{\partial_{\rm rad}^2}{8\mu}\right)\psi_l^{(m+4/9)}(r)=\left(1+i\Delta t\frac{\partial_{\rm rad}^2}{8\mu}\right)\psi_l^{(m+1/3)}(r), \tag{3.18}$$

where the difference matrices are given by

$$\partial_{\rm rbd}^2=\frac{1}{\Delta x^2}\begin{pmatrix} -2 & 1 & & & & \\ 1 & \ddots & \ddots & & & \\ & \ddots & -1 & 0 & & \\ & & 0 & -1 & \ddots & \\ & & & \ddots & \ddots & 1 \\ & & & & 1 & -2 \end{pmatrix} \tag{3.19}$$

and

$$\partial_{\rm rad}^2=\frac{1}{\Delta x^2}\begin{pmatrix} 0 & 0 & & & & \\ 0 & \ddots & \ddots & & & \\ & \ddots & -1 & 1 & & \\ & & 1 & -1 & \ddots & \\ & & & \ddots & \ddots & 0 \\ & & & & 0 & 0 \end{pmatrix}. \tag{3.20}$$

Equation (3.17) can be calculated independently by two processors, since the nonzero elements in the block-diagonal matrix (3.19) are separated into two blocks. The adhesive matrix (3.20) connects the two blocks. In calculations of Eqs. (3.16) and (3.18), it is needed to transfer data on the boundaries between the two processors. However, the amount of data transmission is quite small. Thus, by separating the nonzero elements in the matrix in Eq. (3.19) into many blocks with adhesive operators, calculations can be made on a large-scale parallel computer.

Finally, by solving Eq. (3.6) with the procedures (3.9)–(3.11), the functions $\psi_l^{(m+1)}$ at the next time step t_{m+1} are obtained.

IV. NUMERICAL METHOD

In TDCC calculations of Ps-formation cross sections, the *A*, *B*, and *C* particles are assumed to be the positron, electron, and proton. The wave functions $\psi_{lK}^{JM_J\pi}$ are described numerically on 200×200 grid points in the two-dimensional radial space (R_1,r_1) with the extent of $(R_{\max},r_{\max})$. In the channel expansion (2.3) of the wave functions, the upper limit of the orbital angular momentum $l_{\max}$ is taken to be seven; the maximum number of channels is 36. The TDCC equation (2.7) is solved according to the scheme represented in the preceding section. The time step is $\Delta t=0.05$ a.u.

In the SF representation, the radial part of the total wave function at $t_0=0$ is constructed as the product of the ground-state wave function of the hydrogen and an incoming wave packet for the positron,

$$\chi_{J0}^{JM_J\pi}(R_1,r_1,t_0)=g_{kJ}(R_1)\phi_{1s}^{\rm H}(r_1). \tag{4.1}$$

The wave packet is given by

$$g_{kL}(R)=\frac{1}{(\sigma^2\pi)^{1/4}}\exp\left[-\frac{(R-R_0)^2}{2\sigma^2}\right]h_L^-(kR), \quad (4.2)$$

where $k=\sqrt{2M_1E}$ is the wave number with energy E, R_0 the localization radius of the wave packet at t_0, σ the width of the wave packet, and $h_L^-(kR)=\exp(-ikR)\exp(i\pi L/2)$ an asymptotic Hankel function. Note that the wave packet (4.2) has an energy width of $\Delta E=(1/M_1)k\Delta k$, where $\Delta k\approx\sigma^{-1}$. The initial condition (4.1) is transformed into the BF representation with Eq. (2.13) to substitute into the TDCC equation (2.7).

Positronium-formation cross sections are extracted from solutions of the TDCC equation (2.7) by projecting bound-state wave functions of Ps [22],

$$\sigma_{\rm Ps}=\frac{\pi}{k^2}\sum_J (2J+1)\rho_{\rm Ps}^J, \quad (4.3)$$

with

$$\rho_{\rm Ps}^J=\sum_{nlm}\int {\rm d}\boldsymbol{R}_3|\langle\Psi^{JM_J}(\boldsymbol{R}_1,\boldsymbol{r}_1,t)|\phi_{nlm}^{\rm Ps}(\boldsymbol{r}_3)\rangle_{\boldsymbol{r}_3}|^2, \quad (4.4)$$

where the angle bracket means an integral over $\boldsymbol{r}_3$. In calculation of Eq. (4.4), the total wave-function Ψ^{JM_J} is transformed to the function described in the $(c=3)$ coordinate system in Fig. 1(3) with the Hankel-interpolation method mentioned in the next section.

The calculation is performed with a parallel computing system that consists of five personal computers with Pentium III processors (500 and 800 MHz×4). The computers have been clustered with the software package PVM (parallel virtual machine) which allows a computer network to be used as a virtual parallel computer with distributed memories. Our computer code is organized according to a master-slave model. The master contains input-output and control routines of slave processes and is running on one of the processors. The slave contains a time-evolution calculation routine and runs as identical copies on all of the other processors. Each copy manages calculation of the TDCC equation in a quarter of the two-dimensional radial space. The CPU time of calculations for each partial wave is from several minutes to two hours corresponding to the number of channels in the expansion (2.3). The AlphaServer GS60 at the Institute of Space and Astronautical Science is also used in the scalar computing scheme. The CPU time is about twice for corresponding calculations with the parallel computing system.

V. HANKEL-INTERPOLATION METHOD

We present the Hankel-interpolation coordinate transformation method. In the SF representation, the wave-function $\chi^{(c)JM_J}$ in the $(c=1)$ coordinate is transformed into that in the (3) coordinate.

First, we consider the Fourier transformation of the function $\chi^{(1)JM_J}$ in the position space $(\boldsymbol{R}_1,\boldsymbol{r}_1)$ to the momentum space $(\boldsymbol{P}_1,\boldsymbol{p}_1)$,

$$\hat{\chi}^{(1)JM_J}(\boldsymbol{P}_1,\boldsymbol{p}_1)=\frac{1}{(2\pi)^3}\int d\boldsymbol{R}_1\exp(-i\boldsymbol{P}_1\cdot\boldsymbol{R}_1)\times\int d\boldsymbol{r}_1\exp(-i\boldsymbol{p}_1\cdot\boldsymbol{r}_1)\chi^{(1)JM_J}(\boldsymbol{R}_1,\boldsymbol{r}_1). \quad (5.1)$$

In the SF representation, the momentum- and position-space functions are given by

$$\hat{\chi}^{(1)JM_J}(\boldsymbol{P}_1,\boldsymbol{p}_1)=\sum_{L_1l_1}\hat{\chi}_{L_1l_1}^{(1)JM_J}(P_1,p_1)\mathcal{Y}_{L_1l_1}^{JM_J}(\hat{\boldsymbol{P}}_1,\hat{\boldsymbol{p}}_1), \quad (5.2)$$

$$\chi^{(1)JM_J}(\boldsymbol{R}_1,\boldsymbol{r}_1)=\frac{1}{R_1r_1}\sum_{L_1l_1}\chi_{L_1l_1}^{(1)JM_J}(R_1,r_1)\mathcal{Y}_{L_1l_1}^{JM_J}(\hat{\boldsymbol{R}}_1,\hat{\boldsymbol{r}}_1), \quad (5.3)$$

with the angular momentum function

$$\mathcal{Y}_{Ll}^{JM_J}(\hat{\boldsymbol{a}},\hat{\boldsymbol{b}})=\sum_{Mm}C_{LM,lm}^{JM_J}Y_{LM}(\hat{\boldsymbol{a}})Y_{lm}(\hat{\boldsymbol{b}}). \quad (5.4)$$

In Eq. (5.1), expanding the exponential functions into multipole terms and projecting out the angular momentum functions, we have the radial part of Eq. (5.2),

$$\hat{\chi}_{L_1l_1}^{(1)JM_J}(P_1,p_1)=(-i)^{L_1+l_1}\frac{2}{\pi}\int_0^\infty R_1{\rm d}R_1j_{L_1}(P_1R_1)\times\int_0^\infty r_1{\rm d}r_1j_{l_1}(p_1r_1)\chi_{L_1l_1}^{(1)JM_J}(R_1,r_1), \quad (5.5)$$

where j_l is the spherical Bessel function.

Next, we consider the inverse transformation from the momentum space to the position space,

$$\chi^{(1)JM_J}(\boldsymbol{R}_1,\boldsymbol{r}_1)=\frac{1}{(2\pi)^3}\int {\rm d}\boldsymbol{P}_1\exp(i\boldsymbol{P}_1\cdot\boldsymbol{R}_1)\times\int {\rm d}\boldsymbol{p}_1\exp(i\boldsymbol{p}_1\cdot\boldsymbol{r}_1)\hat{\chi}^{(1)JM_J}(\boldsymbol{P}_1,\boldsymbol{p}_1). \quad (5.6)$$

In the right-hand side, the position vectors $\boldsymbol{R}_1$ and $\boldsymbol{r}_1$ are rewritten with the vectors $\boldsymbol{R}_3$ and $\boldsymbol{r}_3$ in the (3) coordinate system through the relation

$$\begin{pmatrix}\boldsymbol{R}_1\\ \boldsymbol{r}_1\end{pmatrix}=\begin{pmatrix}\alpha & \beta\\ \gamma & \delta\end{pmatrix}\begin{pmatrix}\boldsymbol{R}_3\\ \boldsymbol{r}_3\end{pmatrix}, \quad (5.7)$$

where

$$\alpha=-\frac{m_C}{m_C+m_B}, \quad \beta=-\frac{m_B(m_A+m_B+m_C)}{(m_C+m_B)(m_A+m_B)},$$

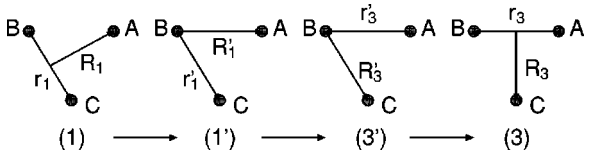

FIG. 2. Three steps of transformation from the (1)-coordinate to the (3)-coordinate system.

$$\gamma=1, \quad \delta=-\frac{m_A}{m_A+m_B}.$$

Substituting the expansions (5.2) and (5.3) into Eq. (5.6) and integrating over the angular variables, we obtain a relation

$$\chi^{(3)JM_J}_{L_3 l_3}(R_3,r_3)=\frac{2}{\pi}R_3 r_3 \sum_{L''l''L'l'L_1 l_1} i^{L''+l''+L'+l'} \times\langle (L''l'')L_1(L'l')l_1 J|(L''L')L_3(l''l')l_3 J\rangle \times\int_0^\infty P_1^2 \mathrm{d}P_1 j_{L''}(\alpha P_1 R_3) j_{l''}(\beta P_1 r_3) \times\int_0^\infty p_1^2 \mathrm{d}p_1 j_{L'}(\gamma p_1 R_3) j_{l'}(\delta p_1 r_3) \times\chi^{(1)JM_J}_{L_1 l_1}(P_1,p_1), \tag{5.8}$$

where

$$\langle (L''l'')L_1(L'l')l_1 J|(L''L')L_3(l''l')l_3 J\rangle =(-)^{L_1+l_1+L_3+l_3}\hat{L}''^2\hat{l}''^2\hat{L}'^2\hat{l}'^2\hat{L}_1\hat{l}_1\hat{L}_3\hat{l}_3 \times\begin{pmatrix} L'' & l'' & L_1\\ 0 & 0 & 0\end{pmatrix}\begin{pmatrix} L' & l' & l_1\\ 0 & 0 & 0\end{pmatrix}\begin{pmatrix} L'' & l' & L_3\\ 0 & 0 & 0\end{pmatrix} \times\begin{pmatrix} l'' & l' & l_3\\ 0 & 0 & 0\end{pmatrix}\begin{Bmatrix} L'' & l'' & L_1\\ L' & l' & l_1\\ L_3 & l_3 & J\end{Bmatrix}, \tag{5.9}$$

with $\hat{l}=\sqrt{2l+1}$. In the left-hand side of Eq. (5.6), we used the identity

$$\chi^{(3)JM_J}(\boldsymbol{R}_3,\boldsymbol{r}_3)=\chi^{(1)JM_J}(\boldsymbol{R}_1,\boldsymbol{r}_1). \tag{5.10}$$

The numerical calculation of Eqs. (5.5) and (5.8) is very hard, since they have double integrals and Eq. (5.8) includes summations over six indices. We consider the three steps of the coordinate transformation through the center-of-mass coordinate systems $(1')$ and $(3')$ illustrated in Fig. 2,

$$\begin{pmatrix}\boldsymbol{R}_1\\ \boldsymbol{r}_1\end{pmatrix}=\begin{pmatrix}1 & \beta_1\\ 0 & 1\end{pmatrix}\begin{pmatrix}\boldsymbol{R}_1'\\ \boldsymbol{r}_1'\end{pmatrix}, \quad \begin{pmatrix}\boldsymbol{R}_1'\\ \boldsymbol{r}_1'\end{pmatrix}=\begin{pmatrix}0 & -1\\ 1 & 0\end{pmatrix}\begin{pmatrix}\boldsymbol{R}_3'\\ \boldsymbol{r}_3'\end{pmatrix},$$

$$\begin{pmatrix}\boldsymbol{R}_3'\\ \boldsymbol{r}_3'\end{pmatrix}=\begin{pmatrix}1 & \beta_3\\ 0 & 1\end{pmatrix}\begin{pmatrix}\boldsymbol{R}_3\\ \boldsymbol{r}_3\end{pmatrix}, \tag{5.11}$$

where

$$\beta_1=-\frac{m_C}{m_B+m_C}, \quad \beta_3=-\frac{m_A}{m_A+m_B}.$$

The three matrices satisfy the identity

$$\begin{pmatrix}\alpha & \beta\\ \gamma & \delta\end{pmatrix}=\begin{pmatrix}1 & \beta_1\\ 0 & 1\end{pmatrix}\begin{pmatrix}0 & -1\\ 1 & 0\end{pmatrix}\begin{pmatrix}1 & \beta_3\\ 0 & 1\end{pmatrix}. \tag{5.12}$$

Equations (5.5) and (5.8) are reduced to a simple form, since one or two of the elements are zero in the three matrices. For the first transformation from the (1) to the $(1')$ coordinate, we have a relation

$$\chi^{(1')JM_J}_{L_1'l_1'}(R_1',r_1')=\frac{\pi}{2}R_1'\sum_{l''L_1l_1} i^{L_1'-L_1} \times\langle (L_1'l'')L_1(0l_1)l_1 J|(L_1'0)L_1'(l''l_1)l_1' J\rangle \times\int_0^\infty P_1^2 \mathrm{d}P_1 j_{L_1'}(P_1R_1') j_{l''}(|\beta_1|P_1 r_1') \times\int_0^\infty R_1 \mathrm{d}R_1 j_{L_1}(P_1R_1)\chi^{(1)JM_J}_{L_1l_1}(R_1,r_1). \tag{5.13}$$

Equation (5.13) can be calculated rapidly by storing values of the spherical Bessel functions into arrays before the calculation. Here, the upper limit of the P_1 integral is taken to be $P_{\max}=\pi/\Delta R_1$ [37,38], where $\Delta R_1=R_{\max}/N$ and N is the number of grid points.

The Hankel-interpolation method surpasses in numerical accuracy in comparison with previous interpolation methods utilizing the Fourier transformation [39,40] and the reduced-rotation matrix [41,42]. In these methods, one needs to interpolate values on several grid points in the initial coordinate function to obtain a value for one grid point in the final coordinate function. This is because the grid points of the initial coordinate do not line up on the finial coordinate. Our method uses the same grid points for all channels. Moreover, the angular part (5.9) is determined by Racah algebra.

VI. RESULTS AND DISCUSSION

Time evolution of wave functions in the SF representation for a positron energy of 30 eV is shown in Fig. 3 [43]; (a)–(c) and (d)–(f) show the $(L,l)=(0,0)$ and $(1,1)$ channels. In this calculation, we take $R_{\max}=r_{\max}=40$ a.u., $\sigma=6$ a.u., and $R_0=20$ a.u. The propagation time of the wave packet is $t_{\max}=27$ a.u., which corresponds 540 time steps. In the figures, the wave densities, square of absolute values of the wave functions, are drown with contours on a logarithmic scale. Figure 3(a) shows the initial condition (4.1) in the (0,0) channel. The shape of the contours is determined by the wave-packet width in the R direction and the ground-state orbital of the hydrogen in the r direction. In the two-dimensional radial space, the incoming wave packet propagates to the origin along the R axis as the time passes. The wave packet is reflected at $r=0$ and becomes an outgoing wave; the wave propagates to the right direction. The outgo-

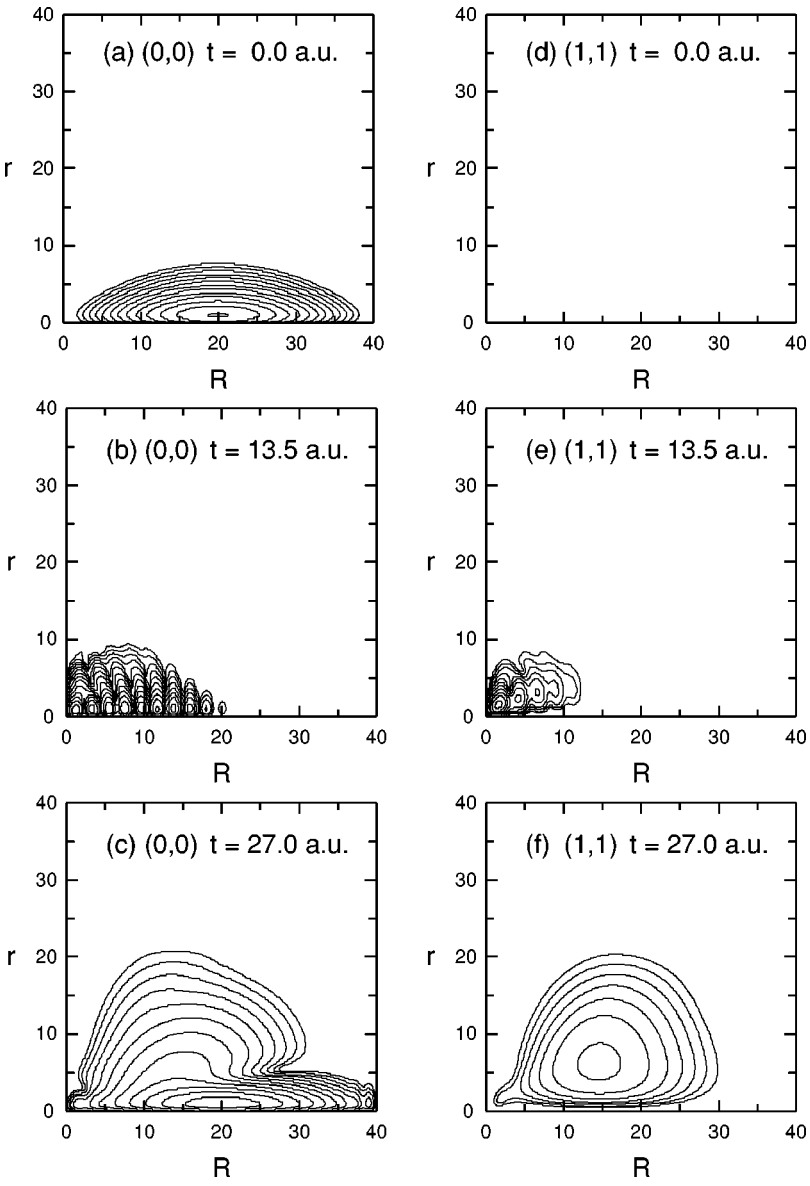

FIG. 3. Time evolution of wave functions at $t=0$, 13.5, and 27.0 a.u. (a), (b), and (c) represent the $(L,l)=(0,0)$ channel and (d), (e), and (f) represent the (1,1) channel. Contours are plotted on a logarithmic scale.

ing wave interferes with the rear component of the incoming wave. In Fig. 3(b), this interference, which is due to quantum effects, is found as many nodes of the contours. In Fig. 3(c) at $t_{\max}$, most components of the wave packet propagate along the R axis. These components represent elastic scattering and excitation to excited bound s states of the hydrogen. A small component that propagates to the right-diagonal direction represents ionization and Ps formation.

In the (1,1) channel, as shown in Fig. 3(d), the wave density is zero at t_0 by the initial condition. In Fig. 3(e), as time increases, a wave emerges in the vicinity of the origin. In Fig. 3(f), the emerging wave becomes a large mound. This is due to the fact that the (1,1) channel is directly coupled with the (0,0) channel through the dipole interaction. The wave includes two components; one of which propagates along the R axis, while the other propagates to the right diagonal direction. The former represents excitation to p states of the hydrogen. The latter represents ionization and Ps formation.

Table I shows contributions of partial waves, $J=0-8$, to Ps-formation cross sections at positron energies of 10, 20, . . . ,50 eV. Here, the upper limit of the electron angular momentum in the channel expansion (2.3) of wave functions has been taken to be $l_{\max}=7$. The partial-wave contributions converge within three percents. Thus, the numerical error caused by the cutoff of partial-wave contributions is sufficiently small. Table II shows convergence of Ps-formation cross sections with increasing $l_{\max}=0-7$, where partial wave contributions of $J=0-8$ are summed at each step of $l_{\max}$. The cross section is quite small for $l_{\max}=0$ and rapidly increases with $l_{\max}$. The convergence of the cross section is slow in comparison with that of the partial-wave contributions; it is, in particular, slow at positron energies higher than 40 eV. We estimate the numerical error caused by the limitation of $l_{\max}$ to be within several percents for energies lower than 30 eV. However, for energies higher than 40 eV, the error is somewhat large and estimated to be about ten percent.

Table III shows the present results of Ps-formation cross sections. In this calculation, we took $R_{\max}=6\sigma$, $r_{\max}=40$

TABLE I. Convergence of Ps-formation cross sections (units of πa_0^2) with respect to the partial wave J.

	E (eV)				
J	10	20	30	40	50
0	0.022	0.013	0.007	0.003	0.001
1	0.499	0.314	0.124	0.048	0.021
2	0.999	0.706	0.304	0.124	0.057
3	0.530	0.705	0.345	0.148	0.070
4	0.194	0.480	0.275	0.125	0.061
5	0.119	0.258	0.173	0.084	0.042
6	0.107	0.123	0.095	0.049	0.025
7	0.096	0.057	0.046	0.025	0.013
8	0.071	0.026	0.021	0.012	0.006
Total	2.636	2.681	1.391	0.617	0.299

a.u., $R_0 = R_{\max}/2$, $\sigma = 3\lambda$ with the de Broglie wave-length $\lambda = 2\pi/k$, and $t_{\max} \geqslant 2R_0/v$ with the velocity v of the wave packet. In Fig. 4, the results are compared with the experiments of Weber *et al.* [3] and Zhou *et al.* [4], and previous calculations which deal with a wide range of positron energy; Schwinger variational calculation by Kar and Mandal [6,44], close-coupling calculations by Mitroy [19] and Kernoghan *et al.* [20], and TDCC calculation by Plante and Pindzola [27]. In positron energies lower than 35 eV, the present results are in excellent agreement with the experiment of Zhou *et al.* For energies higher than 40 eV, the present results somewhat underestimated the measured cross section. This underestimation is due to the limitation of the channel expansion of wave functions discussed above. In comparison with the experiment of Weber *et al.*, all of the results underestimate the experiment. However, the other calculations, except for the TDCC calculation of Plante and Pindzola, agree with the experiment of Zhou *et al.* Their TDCC method is essentially equivalent to our method. However, they made an inconsistent treatment; Ps-formation cross sections were estimated from transfer-ionization (Ps-formation plus ionization) cross sections obtained with the TDCC method by subtracting ionization cross sections calculated with a lowest-order distorted-wave method. The distorted-wave method is not a good approximation for this energy region in which correlation effects are important. Moreover, the number of channels included is small. Thus, their results have large uncertainties. Therefore, we may conclude that in the present calculation, accurate values of Ps-formation cross sections have been obtained with a time-dependent treatment.

TABLE II. Convergence of Ps-formation cross sections (units of πa_0^2) with increasing the upper limit $l_{\max}$ of the electron angular momentum.

	E (eV)				
$l_{\max}$	10	20	30	40	50
0	0.659	0.144	0.048	0.020	0.010
1	0.732	0.273	0.110	0.046	0.024
3	1.650	1.630	0.538	0.283	0.139
5	2.335	2.561	1.220	0.509	0.244
6	2.513	2.673	1.336	0.575	0.277
7	2.636	2.681	1.391	0.617	0.299

TABLE III. Ps-formation cross section.

E (eV)	$\sigma_{\rm Ps}$ (units of πa_0^2)	E (eV)	$\sigma_{\rm Ps}$ (units of πa_0^2)
6.8	0.572	20	2.681
8	1.228	25	1.990
10	2.636	30	1.391
12	3.216	35	0.955
14	3.318	40	0.617
16	3.206	45	0.432
18	2.960	50	0.299

Figure 4 also shows that the present results are more accurate for intermediate energies, 20-40 eV, in contrast to the close-coupling calculation. The results of Mitroy [19] and Kernoghan *et al.* [20] overestimate the cross section for the intermediate energies. It is supposed that this overestimation comes from their treatment of Ps formation of excited states. In their close-coupling calculations, only the $1s$, $2s$, and $2p$ states of Ps were included, while the other states were not included, even if they ware open channels. Ps formation of excited s and p states was taken into account with the n^{-3} scaling law [45]. However, the scaling law is applicable only for highly exited states such as Rydberg states. On the other hand, the Schwinger variational calculation by Kar and Mandal [6,44] is in excellent agreement with the experiment [4] in the whole energy region. However, they took into account only Ps formation of the ground state that was the most important contribution. In the present calculation, Ps formation of excited states is also important at high energies; its contribution amounts to a few tenths of a percent of the Ps-formation cross section.

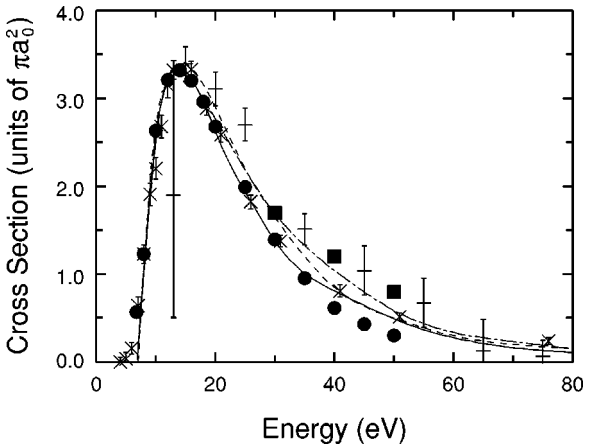

FIG. 4. Ps-formation cross section. Closed circles represent the present calculation (Table III); closed squares, TDCC by Plante and Pindzola [27]; solid line, Schwinger variational method by Kar and Mandal [6,44]; dash-dotted line, 28-state close-coupling by Mitroy [19]; broken line, 33-state close-coupling by Kernohgan *et al.* [20]; pluses and crosses, experiments of Weber *et al.* [3] and Zhou *et al.* [4].

It should be noted that in the present calculation, the cross section does not vanish at the threshold (6.8 eV). This is caused by the use of the wave-packet approximation. The wave packet used at the threshold has an energy width of about 1 eV. This width corresponds to that of positron beam used in the experiment [4]. Therefore, the present calculation has reproduced the experimental result at the threshold.

VII. SUMMARY

We have developed a fast and stable TDCC method and the Hankel-interpolation method to apply to Ps formation in positron-hydrogen collisions. In the TDCC calculation, we showed time evolution of wave packets that described dynamics of positron-hydrogen collisions. The Ps-formation cross sections have been calculated for positron energies of 6.8–50 eV. For energies lower than 35 eV, the present results are sufficiently accurate and in excellent agreement with the experiment by Zhou *et al.* For energies higher than 40 eV, the present calculation somewhat underestimates the experimental results. The present paper has consistently treated Ps formation with the TDCC method and demonstrates usefulness of the method for atomic rearrangement collisions.

ACKNOWLEDGMENTS

We are grateful to Dr. I. Kawata and Dr. A. Ichimura for helpful discussions. We are particularly indebted to Dr. P. Froerich and Dr. H. Kudo for valuable suggestions. We also thank Dr. K. Tanida for supports in development of the cluster computer system. N.Y. acknowledges support from the Japan Society for the Promotion of Science. Y.K. wishes to acknowledge the Grant-in-Aid for Scientific Research, Ministry of Education and Culture, and Inoue Foundation for Science for their generous financial support. The computation was carried out also on the AlphaServer GS60 at the Institute of Space and Astronautical Science.

[1] R. P. McEachran and A. D. Stauffer, in *Atomic Molecular & Optical Physics Handbook*, edited by G. W. F. Drake (American Institute of Physics, New York, 1996).
[2] M. Charlton and J. W. Humberston, *Positron Physics* (Cambridge University Press, Cambridge, 2001).
[3] M. Weber, A. Hofmann, W. Raith, and W. Sperber, Hyperfine Interact. **89**, 221 (1994); W. Sperber, D. Becker, K. G. Lynn, W. Raith, A. Schwab, G. Sinapius, G. Spicher, and M. Weber, Phys. Rev. Lett. **68**, 3690 (1992).
[4] S. Zhou, W. E. Kauppila, C. K. Kwan, and T. S. Stein, Phys. Rev. Lett. **72**, 1443 (1994); S. Zhou, H. Li, W. E. Kauppila, C. K. Kwan, and T. S. Stein, Phys. Rev. A **55**, 361 (1997).
[5] J. W. Humberston, J. Phys. B **17**, 2353 (1984); C. J. Brown and J. W. Humberston, *ibid.* **18**, L401 (1985); J. W. Humberston, P. Van. Reeth, M. S. T. Watts, and W. E. Meyerhof, *ibid.* **30**, 2477 (1997); P. Van. Reeth and J. W. Humberston, *ibid.* **31**, L621 (1998).
[6] S. Kar and P. Mandal, J. Phys. B **30**, L627 (1997); **32**, 2297 (1999).
[7] K. Higgins and P. G. Burke, J. Phys. B **24**, L343 (1991); **26**, 4269 (1993).
[8] G. Liu and T. T. Gien, Phys. Rev. A **46**, 3918 (1992); Y. R. Kuang and T. T. Gien, *ibid.* **55**, 256 (1997).
[9] J. Mitroy, J. Phys. B **26**, 4861 (1993); J. Mitroy and K. Ratnavelu, *ibid.* **28**, 287 (1995); J. Mitroy, Aust. J. Phys. **46**, 751 (1993); **48**, 645 (1995); J. Mitroy, L. Berge, A. Stelbovics, Phys. Rev. Lett. **73**, 2966 (1994).
[10] S. J. Ward, J. H. Macek, and S. Yu. Ovchinnikov, Phys. Rev. A **59**, 4418 (1999).
[11] R. K. Janev and E. A. Solov'ev, J. Phys. B **32**, 3215 (1999).
[12] R. N. Hewitt, C. J. Noble, and B. H. Bransden, J. Phys. B **23**, 4185 (1990); **24**, L635 (1991).
[13] J. Mitroy, J. Phys. B **26**, L625 (1993); J. Mitroy and A. T. Stelbovics, *ibid.* **27**, L55 (1994); **27**, 3257 (1994).
[14] M. T. McAlinden, A. A. Kernoghan, and H. R. J. Walters, Hyperfine Interact. **89**, 161 (1994); A. A. Kernoghan, M. T. McAlinden, and H. R. J. Walters, J. Phys. B **27**, L625 (1994); **28**, 1079 (1995).
[15] T. T. Gien, J. Phys. B **27**, L25 (1994).
[16] N. K. Sarkar and A. S. Ghosh, J. Phys. B **27**, 759 (1994).
[17] A. Igarashi and N. Toshima, Phys. Rev. A **50**, 232 (1994).
[18] Y. Zhou and C. D. Lin, J. Phys. B **27**, 5065 (1994); **28**, L519 (1995); **28**, 4907 (1995).
[19] J. Mitroy, J. Phys. B **29**, L263 (1996); **49**, 919 (1996).
[20] A. A. Kernoghan, D. J. R. Robinson, M. T. McAlinden, and H. R. J. Walters, J. Phys. B **29**, 2089 (1996); C. P. Campbell, M. T. McAlinden, A. A. Kernoghan, and H. R. J. Walters, Nucl. Instrum. Methods Phys. Res. B **143**, 41 (1998).
[21] C. Bottcher, J. Phys. B **14**, L349 (1981); Adv. At. Mol. Phys. **20**, 241 (1985).
[22] W. Ihra, M. Draeger, G. Handke, and H. Friedrich, Phys. Rev. A **52**, 3752 (1995).
[23] M. S. Pindzola, and D. R. Schultz, Phys. Rev. A **53**, 1525 (1996); M. S. Pindzola and F. Robicheaux, *ibid.* **54**, 2142 (1996); F. Robicheaux, M. S. Pindzola, and D. R. Plante, *ibid.* **55**, 3573 (1997); M. S. Pindzola and F. Robicheaux, *ibid.* **55**, 4617 (1997); M. S. Pindzola, D. Mitnik, and F. Robicheaux, *ibid.* **59**, 4390 (1999); M. S. Pindzola, J. Colgan, F. Robicheaux, and D. C. Griffin, *ibid.* **62**, 042705 (2000).
[24] D. O. Odero, J. L. Peacher, D. R. Schultz, and D. H. Madison, Phys. Rev. A **63**, 022708 (2001).
[25] M. S. Pindzola and F. Robicheaux, Phys. Rev. A **57**, 318 (1998); **58**, 4229 (1998).
[26] D. R. Schultz, C. Bottcher, D. H. Madison, J. L. Peacher, G. Buffington, M. S. Pindzola, T. W. Gorczyca, P. Gavras, and D. C. Griffin, Phys. Rev. A **50**, 1348 (1994).
[27] D. R. Plante and M. S. Pindzola, Phys. Rev. A **57**, 1038 (1998).
[28] M. D. Feit, J. A. Fleck,Jr., and A. Steiger, J. Comput. Phys. **47**, 412 (1982); M. D. Feit and J. A. Fleck, Jr., J. Comput. Phys. **78**, 301 (1983); **80**, 2578 (1984).
[29] M. Suzuki, Phys. Lett. A **146**, 319 (1990); **32**, 400 (1991); J. Phys. Soc. Jpn. **61**, 3015 (1992); Phys. Lett. A **165**, 378

(1992); **201**, 425 (1995); K. Umeno and M. Suzuki, **181**, 387 (1993).
[30] A. D. Bandrauk and H. Shen, J. Chem. Phys. **99**, 1185 (1993).
[31] A. Goldberg, H. M. Schey, and J. L. Schwartz, Am. J. Phys. **35**, 177 (1967).
[32] A. Askar and A. S. Cakmak, J. Chem. Phys. **68**, 2794 (1978).
[33] H. Kono, A. Kita, Y. Ohtsuki, and Y. Fujimura, J. Comput. Phys. **130**, 148 (1997).
[34] I. Kawata, H. Kono, and Y. Fujimura, J. Chem. Phys. **110**, 11 152 (1999); I. Kawata and H. Kono, *ibid.* **111**, 9498 (1999).
[35] W. H. Press, S. A. Teukolsky, W. T. Vetterling, and B. P. Flannery, *Numerical Recipes in* FORTRAN, 2nd ed. (Cambridge University Press, Cambridge, MA, 1992).
[36] N. Watanabe and M. Tsukada, Phys. Rev. E **62**, 2914 (2000); J. Phys. Soc. Jpn. **69**, 2962 (2000).
[37] D. Kosloff and R. Kosloff, J. Comput. Phys. **52**, 35 (1983); R. Bisseling and R. Kosloff, *ibid.* **59**, 136 (1985).
[38] Y. Sun, R. C. Mowrey, and D. J. Kouri, J. Chem. Phys. **87**, 339 (1987).
[39] R. S. Judson, D. J. Kouri, D. Neuhauser, and M. Baer, Phys. Rev. A **42**, 351 (1990).
[40] G. D. Billing and N. Marković, J. Chem. Phys. **99**, 2674 (1993); N. Marković and G. D. Billing, *ibid.* **100**, 1085 (1994).
[41] W. H. Miller, J. Chem. Phys. **50**, 407 (1969).
[42] D. Neuhauser, M. Baer, R. S. Judson, and D. J. Kouri, J. Chem. Phys. **93**, 312 (1990); M. Baer, I. Last, and H-J. Loesch, *ibid.* **101**, 9648 (1994).
[43] Animations of time evolution of the wave functions are presented at http://nucl.phys.s.u-tokyo.ac.jp/~yam/tdcc/.
[44] S. Kar and P. Mandal, Phys. Rev. A **59**, 1913 (1999); **62**, 052514 (2000); J. Phys. B **33**, L165 (2000).
[45] K. Omidvar, Phys. Rev. A **12**, 911 (1975).